Characterisation of the ultimate particle size distribution of uniform and gap-graded soils

Xiaoyan ZHANG, MSc, PhD
1.School of Mechanics and Civil Engineering，China University of Mining and Technology, Beijing 100083，China; formerly The University of Hong Kong
2.State Key Laboratory of Geohazard Prevention and Geoenvironment Protection

Béatrice A. BAUDET[*], MSc, PhD
Department of Civil, Environmental and Geomatic Engineering, University College London, U.K.; formerly The University of Hong Kong

Wei HU, PhD
1.Chengdu University of Technology, China
2.State Key Laboratory of Geohazard Prevention and Geoenvironment Protection

Qiang XU
1.Chengdu University of Technology, China
2.State Key Laboratory of Geohazard Prevention and Geoenvironment Protection

[*]Department of Civil, Environmental and Geomatic Engineering,
University College London
Chadwick building
Gower street
London WC1E 6BT
U.K.
b.baudet@ucl.ac.uk

Abstract

The ultimate particle size distribution of uniform and gap-graded soils is examined on specimens of carbonate sand that were subjected to large strains in a ring shear apparatus. The gap-graded soils were seen to retain a memory of their initial grading even at large strains. The particle size distributions were plotted in double logarithmic graphs either by mass or by number computed assuming different shapes. It was not possible to find linear subsets of the data, and since the samples were found experimentally to have converged to an ultimate grading, this suggests that the initial bimodal distribution prevented reaching an ultimate fractal distribution. Plots of the probability density functions of the particle sizes before and after shearing show the evolution of the gap-graded soils from a bimodal to a multi-modal distribution. This is accompanied by an evolution of the shape of the particles, visible in microphotographs and projections of the grains before and after test.

INTRODUCTION

Most soils subjected to compression to high stresses or shearing to large strains suffer particle breakage. The existence of an ultimate grading for soils has been suggested from experimental data, for example by Coop et al. (2004) for uniform sands sheared to large strains, although there were different gradings for different normal stresses, or by Altuhafi et al. (2011) for a natural subglacial till. Turcotte (1986) reported that many granular geomaterials resulting from weathering or fragmentation follow a power law frequency distribution of sizes, also called fractal (Mandelbrot, 1982). This implies that the probability of any size range to break is the same (scale invariance). This concept has been increasingly used in soil mechanics in models for particle breakage (e.g. McDowell and Bolton, 1998; Einav, 2007a; Russell, 2011) or to characterise ultimate particle size distributions (e.g. Altuhafi et al., 2011). It is not clear however that the ultimate grading of atypical soils such as bimodal soils would satisfy fractality.

Two approaches have been reported in the literature, a mass-based approach that uses sieving test data (e.g. Coop et al., 2004; Altuhafi and Coop, 2011), and a number-based approach that computes the number of soil particles from the mass, generally by assuming a constant shape of particles (e.g. Tyler and Wheatcraft, 1989; Hooke and Iverson, 1995; Altuhafi and Baudet, 2011). In the field of soil science, Perfect et al. (1992) showed that for silt loam soils with particles sizes ranging between 0.5 and 30 mm the fractal dimensions computed by number- and mass-based

approaches were the same. The traditional way to describe fractals is by a power law between number and size (Mandelbrot, 1982):

$$N \propto r^{-D} \tag{1}$$

where N is the number of objects with a linear dimension greater than r; the exponent D is defined as the fractal dimension. Turcotte (1986) proposed that the size distribution resulting from fragmentation can be expressed as:

$$N(> m) = C m^{-b} \tag{2}$$

where N(> m) is the number of fragments with a mass greater than m, and C and b are constants, b being equivalent to the fractal dimension. For a material of constant density (or constant specific gravity), the mass is proportional to the volume ($m \propto r^3$), so if the volume is taken simply as r^3 (i.e. no shape is implied), by replacing into (2) and comparing with (1) we obtain:

$$D = 3b \tag{3}$$

The two power law distributions (1) and (2) have been considered equivalent, and several earth scientists (e.g. Sammis et al., 1987; Hooke and Iverson, 1995; Benn and Gemmel, 2002) as well as soil scientists (e.g. Kozak et al., 1996; Grout et al., 1998) have determined the fractal nature of soil particle size distributions from a double logarithmic plot of number of particles against size. The fractal dimensions computed in this manner range between 2 and 3 (Turcotte, 1986; Kozak et al., 1996), with some exceptions: for example Hartmann (1969) reported values of 1.89 for artificially crushed quartz and 3.54 for and ash and pumice. Kozak et al. (1996) noted that while (1) can be used to generate distributions with values of D larger than 3, these

4

distributions contain a majority of fines and do not represent the result from pure fragmentation modelled by Turcotte (1986). It is not uncommon to find such high values in glacial tills which have been created by a mixture of intense crushing and abrasion during shearing underneath glaciers (e.g. Altuhafi et al., 2010; Altuhafi and Baudet, 2011). By comparison, the mass-based approach makes direct use of the sieving test data. For a fractal distribution of particle sizes, the slope of the cumulative mass distribution versus size in a double logarithmic plot is $(3 - D)$ (e.g. Bird et al., 2000). The fractal dimensions determined using this method are around 2.5 for pure sands (e.g. McDowell and Bolton, 1998; Millan et al., 2003; Coop et al., 2004).

Earlier work on the particle size distribution of soils used probabilistic models with lognormal distributions (e.g. Epstein, 1948), which were thought to fit data better than fractals. Millan et al. (2003) showed how using a piecewise fractal model to fit different fractal sets in different size ranges may be better suited to describe granular soils. Miao and Airey (2013) tested a uniform and gap-graded soil (40% small grains) in compression and shearing and found that two fractal dimensions could be defined over two size ranges for each soil, with a cut-off at 75 microns for the uniform soil, which corresponds to the silt sieve size, and at about 150 microns for the gap-graded soil, which corresponded to the size of the small grains. They described the distributions as multifractal, which is perhaps misleading as this should refer to particle size distributions with continuously changing fractal dimensions. Huang and Bradford (1992) defined distributions with distinct fractal subsets as "pseudo-fractals.

Zhang and Baudet (2013) found that gap-graded soils tend to retain the memory of their initial distribution even after compression to high stress, so that the grain size distribution after testing shows a "knee" corresponding to the size of small particles in the gap-graded soil (example shown later in Figure 3). Zhang and Baudet (2015) found that the probability density functions of grain sizes of a uniform and a gap-graded carbonate sand exhibited several peaks over distinct size ranges after shearing. They explored whether there is a correspondence with the distinct fractal sets determined from the number-based distribution but could not reach any firm conclusion. This paper examines the different ways of characterising the ultimate particle size distribution by using data from tests on uniform and gap-graded soils after shearing to very large strains. The data are analysed as cumulative distribution functions by mass and by number, and as probability density functions. A brief assessment of their fractality is given. Additional information is given from analyses of the distribution of particle shapes before and after shearing using probability density functions combined with micrographs and projections of grain images.

MATERIALS AND TESTING PROCEDURES

The tests were carried out on biogenic carbonate sand (CS) from the South China Sea comprising mainly mollusc and foraminifera shells. The sand was first separated into different uniform sizes by mechanical sieving. Six sizes of grains were selected, d_{small} = 0.063-0.15 mm, 0.15-0.212 mm, and 0.212-0.3 mm for the small particles, and d_{large}

= 0.6-1.18 mm, 1.18-2.0 mm, and 2.0-2.36 mm for the large particles. Specimens were prepared with a ratio of large to small particles R kept approximately constant, with R = 8.35, 8.78 and 8.52 for the smaller, medium- and larger-sized samples respectively so the effect of size rather than ratio of sizes could be highlighted. The specimens were prepared at a designed initial grading by mixing small and large particles in exact proportion from 20 to 60% small grains (SG) content. A total of ten tests were carried out, as summarised in Table 1.

In order to study the ultimate particle size distribution of soil by fractal analysis, it is necessary to continue crushing the soil grains until a stable grading is reached. The ring shear apparatus allows reaching very large strains and obtain significant breakage in the soil. Coop et al. (2004) showed, using ring shear test data, that uniform sand reaches a stable fractal distribution upon shearing to large strains, but that it depends on the normal stress level. The ring shear apparatus was also used by Hooke and Iverson (1995) and Altuhafi et al. (2011) to study the fractal distribution of particle sizes in glacial sediments. In this study a ring shear apparatus manufactured by Wille Geotechnik was used to shear the specimens to very large strains.

The apparatus allows a maximum vertical load of 10 kN and a maximum shear load of 7.5 kN to be applied. Two load cells and an electronic dial gauge are used to measure vertical and shear stresses and vertical deformation. The specimens tested were confined between an outer ring of 100 mm diameter and an inner ring of 50 mm diameter. The ring shear cell, 25 mm high, is made of two parts to create a shear zone in the middle. The maximum horizontal travel speed that can be reached by the

apparatus is approximately 180 °/min, which is equivalent to 200 mm/min for an outer diameter of 100 mm, but because Yang et al. (2010) pointed out that fast shearing displacement rates may accelerate particle breakage in the shear zone, the tests presented in this paper were performed with a slower shearing rate of 6 mm/min. Each specimen was sheared under 400 kPa normal stress. Preliminary tests during which the shearing distance was varied showed that the particle size distributions converge to an ultimate grading at a shear distance of 5,200 mm or above (Zhang, 2015).

The particle size distributions of the specimens before testing were determined by two methods, manual sieving and using a dynamic image sensor (Qicpic, Sympatec) where soil particles are put through a vibratory feeder to disperse them before free-falling in front of pulsed light. Particle images are captured by a high speed digital camera (450 frames per second) with a resolution of 1 micron for size and shape characteristics. The Qicpic apparatus gives several measures of size, such as the Feret diameter (distance of two parallel tangents to the contour of the grain), the EQPC (diameter of a circle that has the same area as the projection area of the particle), the dimensions of the minimum bounding rectangle (BR) or the longest/shortest direct path across the grain (LEFI/DIFI), more suited to fibre shapes. Altuhafi and Coop (2011) found that the minimum Feret diameters correspond best to mesh sizes used in manual sieving. The shape of the grains can also be determined from the Qicpic measurements, such as sphericity, calculated as the ratio of the perimeter of the grain to that of the circle of equivalent surface area, convexity,

calculated as the ratio of the surface area of the grain to the area of the convex Hull surface, aspect ratio, calculated as the ratio between the minimum and maximum Feret diameters, or elongation, the ratio DIFI/LEFI. The specimens after testing were first wet sieved to separate coarse and fine particles, then the particle size distribution was determined by combining gradings found by manual sieving or using the Qicpic apparatus for particles larger than 63 microns, and that found by using a Malvern Mastersizer 2000 particle size analyser for smaller particles. Scanning electron microscopy of some samples before and after testing also gave some insight into the surface structure of the particles and the minimum size obtained through comminution. In Figure 1, there is evidence of internal voids in the grains that are in contact with the surface, giving it a dimpled aspect.

DETERMINATION OF THE PARTICLE SIZE DISTRIBUTION AFTER SHEARING

During ring shear testing intense crushing around the shearing plane caused interlocking of the broken particles, creating a finite solid "ring" of crushed soil ("zone 2") from which the top ("zone 1") and bottom ("zone 3") layers of the sample could easily be brushed away. This is similar to what was found by Coop et al. (2004), Altuhafi et al. (2011) or Yang et al. (2010) and Ho et al. (2011). The thickness of the shear band is usually found to be a multiplier of the mean grain size (e.g. Ho et al., 2010). The data in Figure 2a do not show any strong influence of the small grains

9

content, with only a slight decrease in thickness until a minimum value for 40% small grains, which could correspond to the maximum packing of the mixture. With the same ratio of large to small particles in the tested specimens, there appears to be a weak relation between the shear band thickness and size of particles.

Only soil retrieved in the finite shear band of the specimen was sieved for analysis, following Coop et al.'s (2004) recommendation on how to monitor soil particle breakage in ring shear tests. The evidence that all the significant breakage occurred in zone 2 is demonstrated by the particle size distribution (Figure 2b) and cumulative distribution of the particle shape (Figure 2c) determined before and after testing. The data obtained by sieving are shown for specimen R1.18/8.35-40 as example. The grading obtained by Qicpic for zone 2 using the minimum Feret diameters is also shown. There is a small tendency for the Qicpic data to measure larger values for the bigger particles, similarly to what was found by Altuhafi and Coop (2011). The gradings and the aspect ratios in zones 1 and 3 were not affected during shearing. In zone 2, the particle size distribution was seen to move upwards while the aspect ratio was observed to increase by about 7% with the breakage, indicating that the particles were abraded and became more regular with shearing.

In the following, the data from the tests on specimens prepared with coarse particles of size 0.6-1.18 mm are used for illustration; the other specimens were found to show a similar behaviour. Figure 3 shows the cumulative distribution functions of the particle sizes in specimens with 0, 20 and 40% small grains content before and after testing, the latter measured by Qicpic and Malvern Supersizer. The existence of a

"knee", which was highlighted by Zhang and Baudet (2013) in the distribution of gap-graded soil specimens after one-dimensional crushing, and also found by Zhang and Baudet (2015) in specimens prepared with $d_{large} = 2\text{-}2.36$ mm after shearing, is less pronounced but still apparent, owing to the fact that the number of small particles cannot be less than the initial small grains number. The knee would therefore be more obvious at larger numbers of small grains. The distribution of aspect ratio after shearing is shown in Figure 4. For particles larger than 63 microns, the aspect ratio is virtually constant, equal to about 0.72 (values for the larger particles are thought to be biased because of their very small number), while for the smaller particles the values of aspect ratio tend to reduce with size to about 0.6.

Evolution of particle shape

The evolution of the particles' shape during shearing might offer some insight into the crushing mechanism. Figure 5 shows the probability density functions of the aspect ratio, sphericity and convexity before and after testing. The distribution of aspect ratios (fig. 5a) shifts slightly to the right, with the mean aspect ratio increasing from about 0.75 to 0.85. The distribution of sphericities becomes narrower, with a barely discernible increase in mean value (fig. 5b), while the distribution of convexities becomes wider with also barely any shift in mean value (fig. 5c). The aspect ratio is likely to be affected by particle breakage such as splitting in the middle, leading to the particles being less elongated, while the convexity is most likely to be affected by breakage at the asperities e.g. abrasion. The sphericity is usually also sensitive to

11

changes in the particle morphology and the narrowing of the distribution may be a result of the smoothening of the surfaces, as shown in micrographs of grains after testing (figs. 6a & 6b) where the dimpled aspect seen in Figure 1 on grains before testing is no more visible. Figure 6c shows the presence of many very small particles, from 50 microns to less than 1 micron, which are probably the product of abrasion of the honeycomb. These small particles appear to be angular, and from Figure 4 we know they tend to have low aspect ratios. The evolution of aspect ratio, sphericity and convexity in Figure 5 thus captures the tendency for the large particles to become smoother and rounded during shearing, but it is not representative of the very small particles, which represent a small volume of the sample. These small angular particles are likely to be the product of abrasion.

The breakage of the asperities by abrasion is also evident in the projected images of particles of similar size taken from specimens prepared with 40% small grains before (fig. 7a) and after (fig. 7b) test. For example, the convexity of particle no. 2258 (fig. 7a; the particle number refers to the order in which the particles are recorded by QicPic), recorded before shearing, is 0.914 while a similar particle after shearing has a higher convexity of 0.956 (particle no. 628, fig. 7b). On closer inspection of the particles after testing by increasing the magnification (fig. 8), it becomes evident that a substantial number of extremely fine particles are created during shearing in the gap-graded specimens prepared with 20% small grains. It is thought that some of the surface voids visible in the dimpled texture of the particles (fig. 1) are released into very small grains of the order of 1 micron or even smaller.

Determination of the fractal dimension: effect of shape

The fractal dimension is increasingly used for modelling soil crushing (e.g. McDowell and Bolton, 1998; Einav, 2007a; Russell, 2011). Einav (2007a) proposed the following fractal model to simulate the ultimate particle size distribution by mass reached by uniform sand:

$$F_u(d) = \frac{M_d(\Delta < d)}{M_{total}} = \frac{d^{3-D} - d_m^{3-D}}{d_M^{3-D} - d_m^{3-D}} \tag{4}$$

where d represents the size of particles, M is the mass of an assembly of particles, and D is the fractal dimension. The sizes d_m and d_M represent the bounding values of the size interval, with d_M the largest size, and d_m the smallest size. While taking the latter as zero would simplify equation (4), as suggested by Einav (2007a) in his theoretical paper, when applying in practice it is usually the case that the comminution limit is the smallest measured particle size. In his subsequent paper focusing on practical applications Einav (2007b) used 1.4 mm based on experimental sieve data. $F_u(d)$ was compiled from the number-based definition of fractal distributions, with the mass for each size range calculated by multiplying the number of grains in that range by the mass of the individual grains of that size. The specific gravity of the soil was assumed to be constant and the volume of the grains was taken as a sphere i.e. $\frac{\pi}{6}d^3$ (Einav, 2007a). The shape factor ($\frac{\pi}{6}$) occurring on both numerator and denominator in (4), it cancels out so that the formulation of $F_u(d)$ is independent of particle shape. When compiling a number-based distribution of particle sizes however, the usual assumption that particles

are spherical might lead to discrepancies between the fractal dimensions determined using that method and that using the mass cumulative particle size distribution.

The number of particles for the specimens prepared uniform and with 40% small grains (R1.18/1-0 and R1.18/8.35-40) was computed from the measured sieved mass by following Zhang and Baudet's (2013) approach (fig. 9). Two different shapes were assumed, a spherical shape and an ellipsoid shape. The ellipsoid was adopted after seeing the fairly uniform distribution of aspect ratios in Figure 4 over the size range 0.1-1 mm. The equations to find the number of particles $N(d_1,d_2)$ and mean size d_{mean} within a size range d_1-d_2 (expressed in (5) and (6) for spherical particles; after Zhang and Baudet, 2013) were modified to account for the shape. The diameter of the spheres and the short axis of the ellipsoids were taken equal to the minimum Feret diameter. The relevant aspect ratio (AR) for each size range, which is taken as the ratio of between short and long axis of an ellipsoid, was used. The modified equations are given as (7) and (8):

$$N(d_1,d_2) = \frac{6M(d_1,d_2)(D-3)}{\rho \pi D} \frac{d_1^{-D} - d_2^{-D}}{d_1^{3-D} - d_2^{3-D}} \tag{5}$$

$$d_{mean} = \left(\frac{6M(d_1,d_2)}{N(d_1,d_2)\pi \rho} \right)^{\frac{1}{3}} \tag{6}$$

$$N(d_1,d_2) = \frac{3M(d_1,d_2)(D-3)}{4AR\rho \pi D} \frac{d_1^{-D} - d_2^{-D}}{d_1^{3-D} - d_2^{3-D}} \tag{7}$$

$$d_{mean} = \left(\frac{3M(d_1,d_2)}{4AR\,N(d_1,d_2)\pi \rho} \right)^{\frac{1}{3}} \tag{8}$$

14

where $M(d_1,d_2)$ is the mass of soil retained between sieve sizes d_1 and d_2, and ρ is the soil density.

In Figure 9, the number of ellipsoidal particles in the uniform specimen R1.18/1-0 is about six times smaller than the number of spherical particles. The shift downwards is attributed to the larger sizes of the ellipses, and it is also observed that the data shifted slightly towards the right. For the gap-graded specimen (R1.18/8.35-40), the same downward shift is observed, with the number of ellipsoidal particles about 5.8 smaller than the number of spherical particles, and a slight leftward shift is also observed. The different magnitudes of the shifts, and their opposite directions, would suggest that they are not an artefact of the equations. The slope however has remained virtually the same and therefore so does the fractal dimension. Using a slightly different method Perfect et al. (1992) also showed that assuming a spherical or cubic shape of grains should result in the same number-derived fractal dimension i.e. the same slope in the graph. The presence of small grains only seems to affect the number of particles which are smaller than 63 microns, the data points between the grains larger than 63 microns in the two specimens being very close.

Comparison between mass- and number-based approach to characterize the particle size distribution

Figure 10a shows the cumulative mass distribution obtained by sieving of the tested uniform specimens (R1.18/1-0, R2.0/1-0 and R2.36/1-0). There does not seem to be a unique straight line which would characterize any of the distributions over the

15

whole data range. Figure 10b shows the number of particles determined from the mass using (5). Even if showing better alignment, it is still difficult to identify a unique straight line to describe each distribution. The linearization is least possible for the larger particles (0.1-1mm), even though the aspect ratio after shearing seems to remain constant at 0.72 (fig. 4), however for the smaller particles (0.01-0.1mm), while the aspect ratio varies in the range 0.6-0.7 (fig. 4), linearizing would be more possible. The figures show that the specimens with larger particles suffer marginally more breakage in the small size region (data points for R2.36/1-0 plotting the highest, data for R1.18/1-0 the lowest in figure 10a), despite their similar ratios of grain sizes.

An example of linearization is given below. The data are separated into two subsets, following the suggestion that particle size distributions are (pseudo-)fractal over different data ranges (Huang & Bradford, 1992). One fine subset is defined for grains smaller than 45 microns, and one coarse subset for grains larger than 45 microns. By fitting power laws (straight lines in a double logarithmic plot), it is found that the number-based method tends to give lower values of fractal dimension (noted as D_n) than the mass-based method (dimension noted as D_m), particularly in the larger-sized specimens (fig. 10c). One reason might be the small numbers of particles falling within those size ranges that are used in the calculation. Unlike the soil tested by Perfect et al. (1992), who also compared both approaches, the carbonate sand presented here contains internal voids, in particular the larger particles which are closer to intact shells (Figure 1a). The smaller particles are likely to result from fragmentation and therefore will have less internal voids. Frossard et al. (2012) suggested that larger particles have a

16

higher probability of containing internal flaws. This implies that in the larger grains, a more open internal structure should give a lower mass for a given number of particles, although it was also found that the number-counting results were highly dependent on how many particles could be captured by the camera and therefore tended not to be repeatable. When adding 40% small grains however, it becomes more difficult to identify any linear trend over any subset, whether from the mass cumulative (fig. 11a) or the number-based distribution (fig. 11b), suggesting that the data cannot be analysed as pseudo-fractals.

POSSIBLE CRUSHING SCENARIOS

A possible scenario leading to the particle size distribution seen in Figure 3 is if the two size fractions (large and small grains) within a gap-graded soil tend towards their fractal grading upon crushing. Following Russell's (2010) approach to describe double porosity with two separate fractal distributions over two volume fractions, the particle size distribution expressed by combining the two fractal gradings using (4) for each size with the relevant proportion of small grains:

$$F_u(d) = SG \times F_{u,small} + (1-SG) \times F_{u,l\arg e} \tag{9}$$

where SG is the small grains content, $F_{u,small}$ and $F_{u,large}$ are the fractal gradings that the fine and coarse fractions would reach eventually, and are expressed by (4) with the relevant values of fractal dimension, D, and bounding values, d_m and d_M. Thus for each fractal subset d_m and d_M are different. The ranges d_m to d_M may either overlap e.g. if d_m

is the same for each subset, or be discontinuous is d_M for the fine subset is smaller than d_m for the coarse subset.

Figure 12 shows predicted and experimental data for gap-graded specimens R1.18/8.35-20 and R1.18/8.35-40, with 20% and 40% small grains contents respectively. The calculation requiring values of fractal dimension to define $F_{u,small}$ and $F_{u,large}$, linear trends were approximated in the same two regions as identified for the uniform specimens: a region for grains smaller than 45 microns and a region for grains larger than 45 microns. This also follows the suggestion by Miao and Airey (2013) that gap-graded soils can be described by two fractal dimensions, although they delimited their regions at the size of the small grains. The analyses were made using the determined value for D_n, as that approach (number-based) proved to provide a slightly better linear fit. The bounding values for each subset influence the predicted curves, and while d_M is easily determined, the value of d_m is not as straightforward. When predicting the evolution of the particle size distribution of silica sand Einav (2007b) used d_m equal to the smallest size found in the sieving analysis, which in that case was 1.4 mm. Another logical choice would be the comminution limit. Among the values suggested by researchers are the size of the minerals elements of the particles, which in quartz would correspond to about 1 micron (Glazner and Mills, 2012), or the critical diameter calculated from Griffith's energy criterion (1921) below which cracking under compression is impossible and yielding occurs (Kendall, 1978). It has also been proposed that the comminution limit is reached when the slope of the normal compression line reduces in plots of specific volume against the logarithm of the

18

vertical effective stress, which occurs at very high stresses (e.g. McDowell and Bolton, 1998; Altuhafi and Coop, 2011). Vilhar et al. (2013) found from high precision particle size analysis that the grading curves of a lime-rich sand converged at about 1 micron after compression to high pressure. In the gap-graded soils tested here, scanning electron microscope images taken from specimens after testing reveal the presence of particles of the order of 1 micron, and even smaller, as seen in Figure 6. Here d_m was taken as 0.1 micron for the smaller grains in each fraction.

The agreement between the predicted curve and the experimental data is not particularly good for either specimen, especially at smaller grain sizes. The analyses predict the "knee" but not at the right value of grain size, and lower than the experimental data. This indicates that the simple assumption of cumulating the two fractal curves for the two size fractions is not enough to replicate the soil behaviour. It could be argued that insufficient shearing was achieved experimentally in order to reach the ultimate grading for each fraction, but it is more likely due to the complex interaction between grains of different sizes, the smaller particles providing some cushioning to the larger ones.

The probability density function, which carries valuable information on the dominant sizes emerging upon crushing, was computed from the Qicpic measurements which have the advantage of being continuous (Figure 13). The distributions evolve from being unimodal (for the uniform soil) to bimodal, and from being bimodal (for the gap-graded specimens) to being tri-modal. Bird et al. (2009) developed different fragmentation models to study the evolution of the particle size distribution according

19

to different scenarios. They found that crushing leads to a lognormal distribution if the probability of breakage of particles reduces with their decreasing size, which implies a relaxation of the scale invariance implicit in fractal distributions. By varying their model, Perfect et al. (1992) also found that power law (i.e. fractal) distributions are generated by fragmentation if there is a threshold size below which crushing cannot occur, which is equivalent to saying that there is a comminution limit. With a bounding value of fragment size, a particle size distribution initially unimodal evolves to becoming bimodal as more grains are created that cannot be broken and the grains at the comminution limit will eventually dominate the distribution. McDowell and Bono (2013) showed that including a limiting comminution size in discrete element simulations of one-dimensional compression causes the compression curve to change curvature at high stresses as well as causing more large particles to break as unbreakable grains are created. This could explain the shift to the left of the coarse particles peak. The experimental data shown in Figure 13 however indicate that while there are very small particles created during shearing, they also contribute to cushioning and hinder further breakage, the majority of the smaller grains being of the order of 20-30 microns. Their angularity (fig. 6) further suggests that they are not affected by crushing even at large strains. The convergence of the particle size distribution towards a multi-modal distribution therefore seems to indicate that the mode of crushing is influenced by the existence of a comminution limit, but the complex interaction between particles of different sizes restricts the fragmentation so that a memory of the initial grading is also retained.

CONCLUSIONS

This paper has used results from ring shear tests conducted on uniformly graded and gap-graded carbonate sand to show that:

(a) Gap-graded soils retain a memory of their initial grading even at large strains. In both uniform and gap-graded soils a significant number of particles smaller than 45 microns. While the larger grains become smoother and slightly less elongated during shearing, as a result of splitting and abrasion, the newly created small grains tend to be angular with more irregular shapes.

(b) The ultimate grading of uniform specimens can be described by two pseudo-fractals. While assuming different shapes e.g. spheres or ellipsoids does not affect the fractal dimension determined by the number-based approach, there are differences between the fractal dimensions determined by mass- or number-based which are attributed to the internal voids within the sand grains.

(c) The gap-graded specimens reach ultimate gradings that are not linear over any subset in double logarithmic plots. It is also not possible to simulate their crushing by assuming that each fraction tends to an ultimate fractal grading. This is attributed to the memory of the initial grading, with a constraint at the "knee" of the distribution, and to cushioning by the smaller particles, preventing further breakage towards a comminution limit.

ACKNOWLEDGMENT

REFERENCES

Altuhafi, F., Baudet, B.A., Sammonds, P., 2010. The mechanics of subglacial sediment: an example of 'transitional behaviour'. Canadian Geotechnical Journal 47(7), 775-790.

Altuhafi, F., Baudet, B.A., 2011. A hypothesis on the relative roles of crushing and abrasion in the mechanical genesis of a glacial sediment. Engineering Geology 120, 1-9.

Altuhafi, F., Coop, M., 2011. Changes to particle characteristics associated with the compression of sands. Géotechnique 61(6), 459-471.

Altuhafi, F., Baudet, B.A., Sammonds, P., 2011. On the particle size distribution of a basaltic till. Soils and Foundations 51(1), 113-121.

Benn, D.I., Gemmell, A.M.D., 2002. Fractal dimensions of diamictic particle-size distributions: simulations and evaluation. Geol. Soc. Am. Bull. 114(5), 528-532.

Bird, N.R.A., Perrier, E., Rieu, M., 2000. The water retention function for a model of soil structure with pore and solid fractal distributions. Eur. J. Soil Sci. 51, 55-63.

Bird, N.R.A., Watts, C.W., Tarquis, A.M., Whitmore, A.P., 2009. Modeling dynamic fragmentation of soil. Vadose Zone J. 8(1), 197-201.

Coop, M.R., Sorensen, K.K., Freitas, T.B., Georgoutsos, G., 2004. Particle breakage during shearing of a carbonate sand. Géotechnique 54(3), 157-163.

Einav, I., 2007a. Breakage mechanics—Part I: Theory. Journal of the Mechanics and Physics of Solids 55(6), 1274-1297.

Einav, I., 2007b. Breakage mechanics—Part II: Modelling granular materials. Journal of the Mechanics and Physics of Solids 55(6), 1298-1320.

Epstein, B., 1948. Logarithmico-normal distribution in breakage of solids. Ind. Eng. Chem. 40, 2289-2291.

Frossard, E., Hu, W., Dano, C., Hicher, P-Y., 2012. Rockfill shear strength evaluation: a rational method based on size effects. Géotechnique 62(5), 415-427.

Glazner, A.F., Mills, R.D., 2012. Interpreting two-dimensional cuts through broken geologic objects: Fractal and non-fractal size distributions. Geosphere 8(4), 902-914.

Griffith, A.A., 1921. VI. The Phenomena of Rupture and Flow in Solids. Philosophical Transactions of the Royal Society of London. Series A, Biological sciences 221, 163-198.

Grout, H., Tarquis, A.M., Wiesner, M.R., 1998. Multifractal Analysis of Particle Size Distributions in Soil. Environmental Science & Technology 32(9), 1176-1182.

Hartmann, W.K., 1969. Terrestrial, lunar and interplanetary rock fragmentation. Icarus 10, 201-213.

Ho, T., Jardine, R., Anh-Minh, N., 2011. Large-displacement interface shear between steel and granular media. Géotechnique, 61(3), 221-234.

Hooke, R.LeB., Iverson, N.R., 1995. Grain size distribution in deforming subglacial tills: role of grain fracture. Geology 57-60.

Huang, C., Bradford, J.M., 1992. Applications of a laser scanner to quantify soil microtopography. Soil Sci. Soc. Am. J. 56, 14-21.

Kendall, K., 1978. The impossibility of comminuting small particles by compression. Nature 272710-711.

Kozak, E., Pachepsky, Ya. A., Sokolowski, S., Sokolowska, Z., Stepniewski, W., 1996. A modified number-based method for estimating fragmentation fractal dimensions of soils. Soil Sci. Soc. Am. 60, 1291-1297.

Mandelbrot, B.B., 1982. The fractal geometry of nature. W.H. Freeman, San Francisco.

McDowell, G.R., Bolton, M.D., 1998. On the micromechanics of crushable aggregates. Géotechnique 48(5), 667 –679

McDowell, G.R., DeBono, J.P., 2013. On the micro mechanics of one-dimensional normal compression. Géotechnique 63(11), 895-908.

Miao, G., Airey, D., 2013., Breakage and ultimate states for a carbonate sand. Géotechnique 63(14), 1221-1229.

Millán, H., González-Posada, M., Aguilar, M., Domínguez, J., Céspedes, L., 2003. On the fractal scaling of soil data. Particle-size distributions. Geoderma 117(1–2), 117-128.

Perfect, E., Rasiah, V., Kay, B.D., 1992. Fractal Dimensions of Soil Aggregate-size Distributions Calculated by Number and Mass. Soil Sci. Soc. Am. J. 56(5), 1407-1409.

Russell, A.R., 2010. Water retention characteristics of soils with double porosity. European Journal of Soil Science 61, 412-424.

Russell, A.R., 2011. A compression line for soils with evolving particle and pore size distributions due to particle crushing. Géotechnique Letters 1, 5-9.

Sammis, C., King, G., Biegel, R., 1987. The kinematics of gouge deformation. PAGEOPH 125(5), 777-812.

Turcotte, D.L., 1986. Fractals and Fragmentation. J. Geophys. Res., 91(B2), 1921-1926.

Tyler, S.W., Wheatcraft, S.W., 1989. Application of fractal mathematics to soil water retention estimation. Soil Sci. Soc. Am. J. 53, 987-996.

Vilhar, G., Jovičić, V., Coop, M.R., 2013. The role of particle breakage in the mechanics of a non-plastic silty sand. Soils and Foundations 53(1), 91-104.

Yang, Z.X., Jardine, R.J., Zhu, B.T., Foray, P., Tsuha, C.H.C., 2010. Sand grain crushing and interface shearing during displacement pile installation in sand. Géotechnique 60(6), 469-482.

Zhang, X., 2015. Particle breakage in uniform and gap-graded soils. PhD thesis, The University of Hong Kong.

Zhang, X. , Baudet, B. A., 2013. Particle breakage in gap-graded soil. Géotechnique Letters 3(2), 72-77.

Zhang, X., Baudet, B.A. 2015. The multi-fractal nature of soil particle size distribution. Geomechanics from Micro to Macro, Soga et al. (Eds), 1183-1188. Proc. IS-Cambridge, 1-3 Sept. 2014. Taylor & Francis Group, London.

Table 1 Summary of the tests used in the analyses

| Tests No.	Ratio	Small size d_{small} (mm)	Large size d_{large} (mm)	SG content (%)
R1.18/1-0-3	Uniform	N/A	0.6-1.18	N/A
R2.0/1-0	Uniform	N/A	1.18-2.0	N/A
R2.36/1-0*	Uniform	N/A	2.0-2.36	N/A
R1.18/8.35-20	8.35	0.063-0.15	0.6-1.18	20
R1.18/8.35-40	8.35	0.063-0.15	0.6-1.18	40
R2.0/8.78-20	8.78	0.15-0.212	1.18-2.0	20
R2.0/8.78-40	8.78	0.15-0.212	1.18-2.0	40
R2.36/8.52-20*	8.52	0.212-0.3	2.0-2.36	20
R2.36/8.52-40*	8.52	0.212-0.3	2.0-2.36	40
R2.36/8.52-60*	8.52	0.212-0.3	2.0-2.36	60

*test data used in Zhang and Baudet (2015)

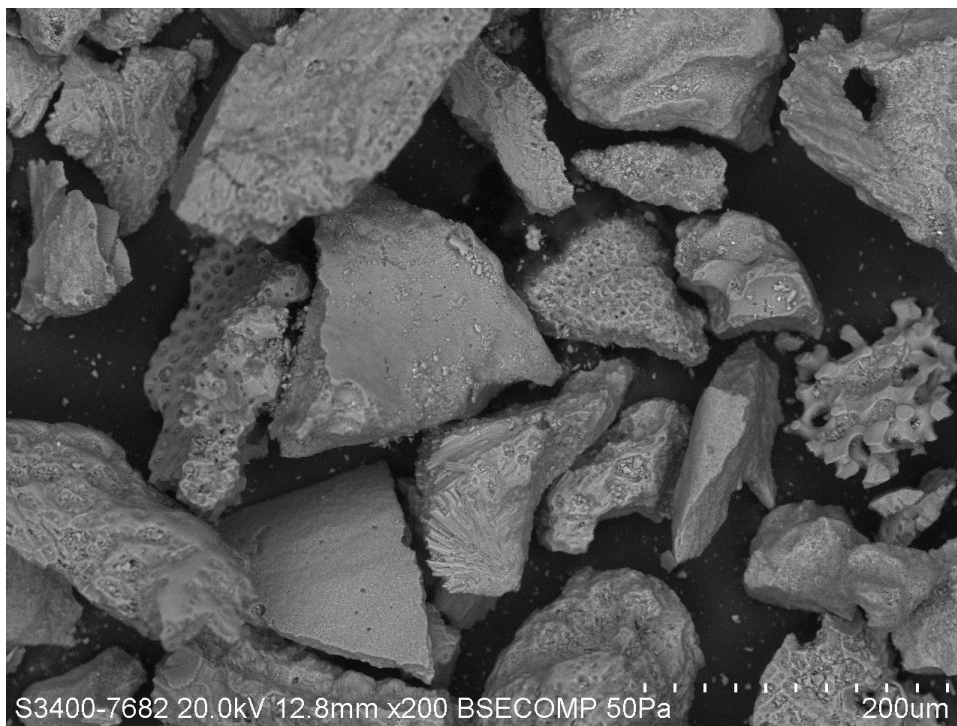(a)

S3400-7674 20.0kV 12.0mm x45 BSECOMP 50Pa   1.00mm
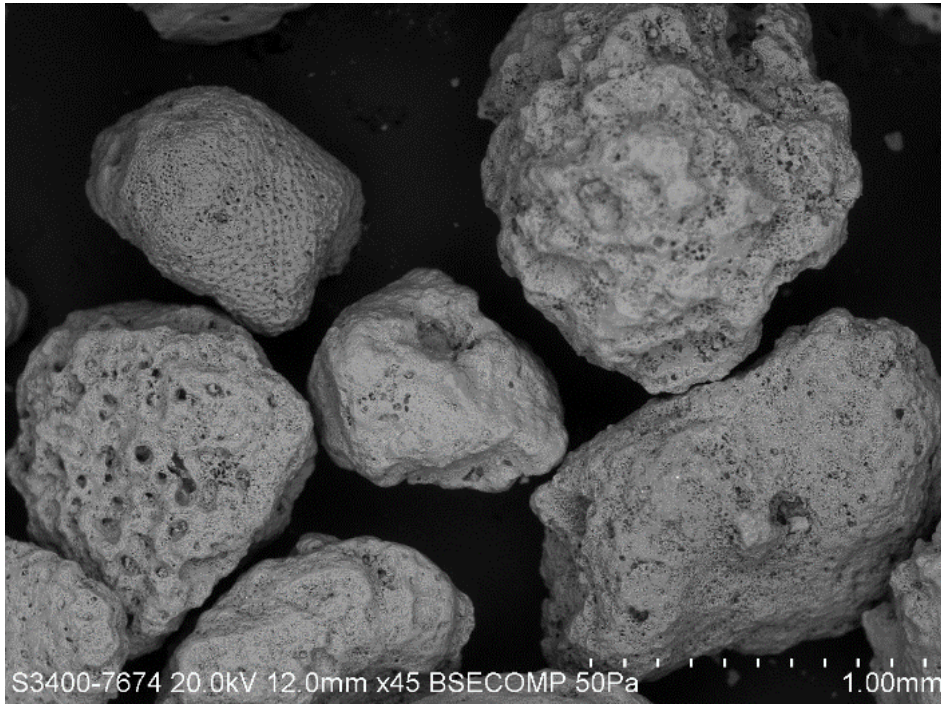
(b)
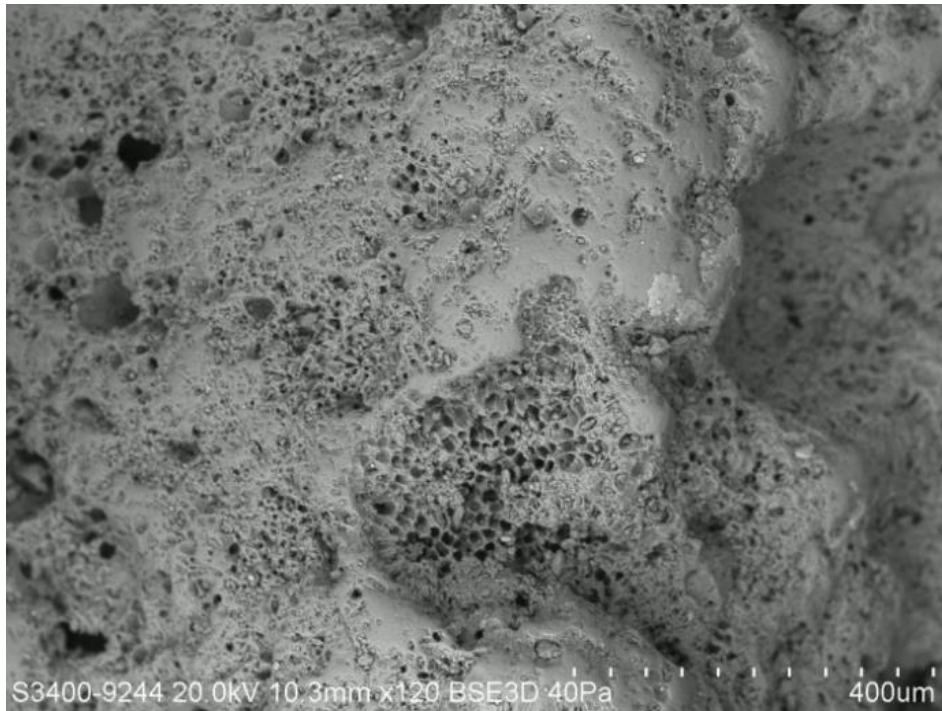
(c)

(d)

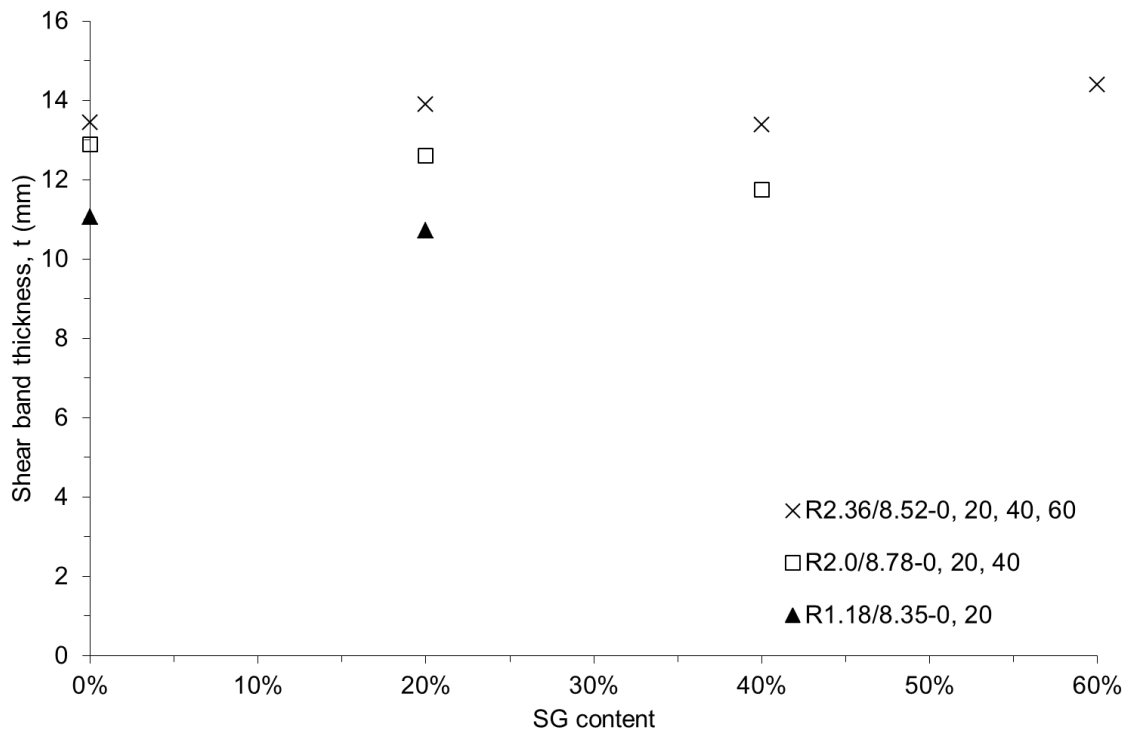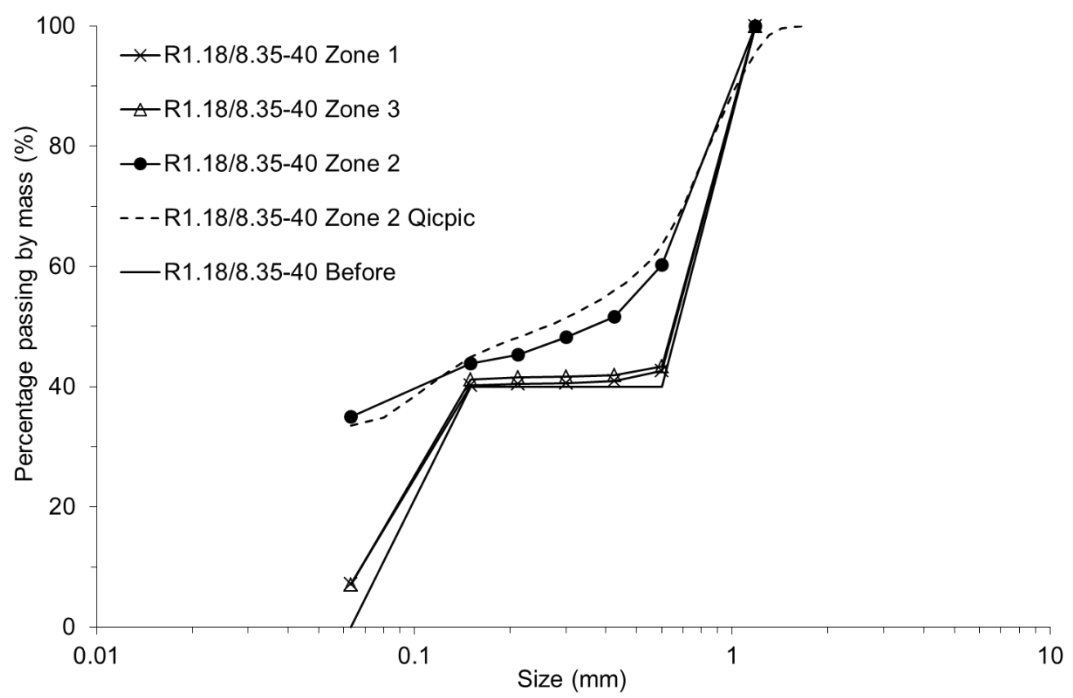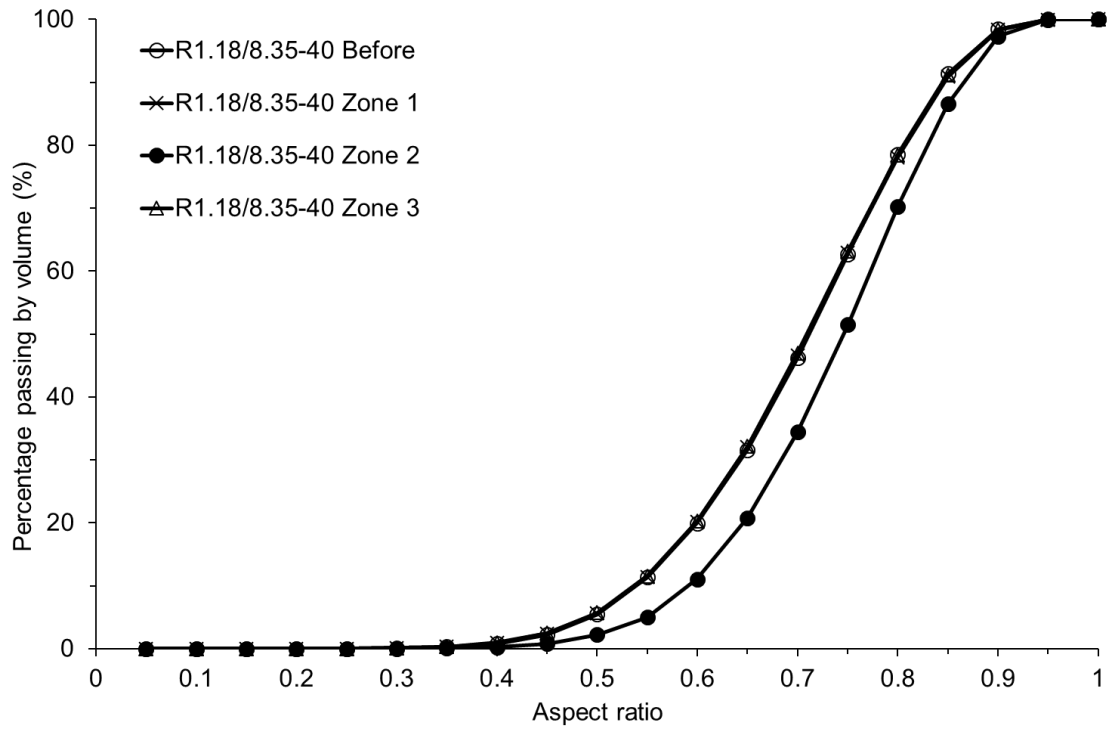**Figure 1** (a) Photograph of soil particles of size 0.6-1.18mm before testing. (b) to (d) Scanning electron micrographs: (b) & (c) grains of 0.6-1.18mm before testing (Hitachi S4800FEG); (d) grains of 0.063-0.15 mm before testing (Hitachi S3400FEG)

(a)

(b)

(c)

Figure 2 Ring shear test data for uniform and gap-graded specimens (a) influence of small grains on the thickness of the shear band; (b) cumulative particle size distribution (by sieving and Qicpic) and (c) cumulative distribution of aspect ratios before and after testing in the three different zones (by Qicpic)
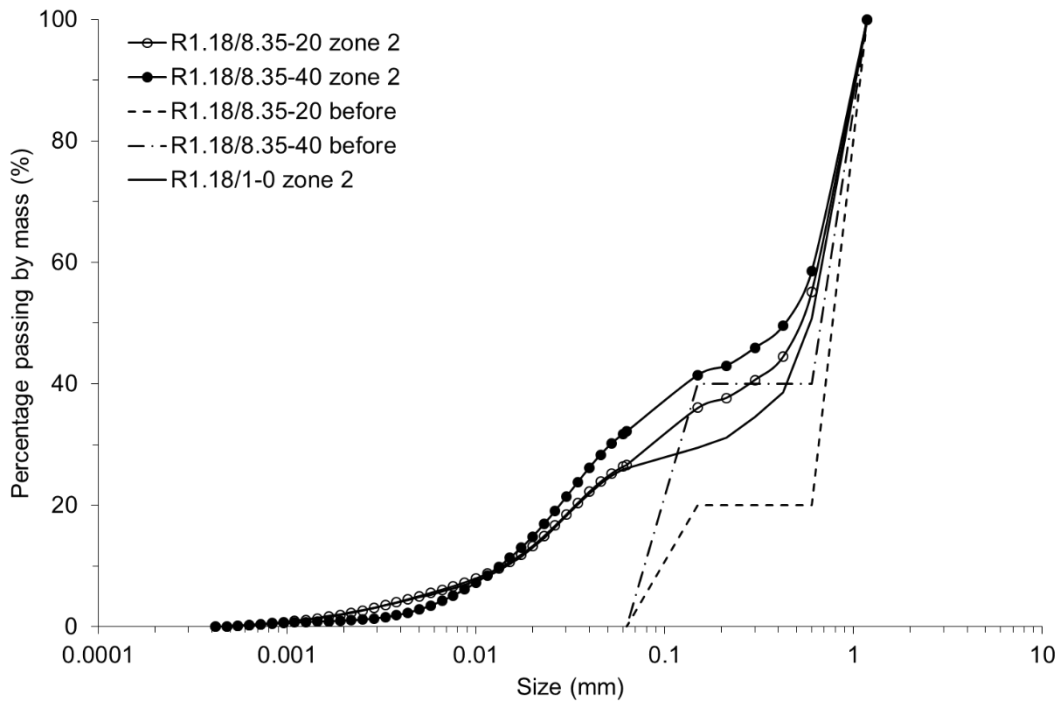
Figure 3 Cumulative distributions of particle sizes before and after testing for gap-graded specimens with d_{large} = 0.6-1.18mm and 20% or 40% small grains content (by Qicpic and Malvern Supersizer)

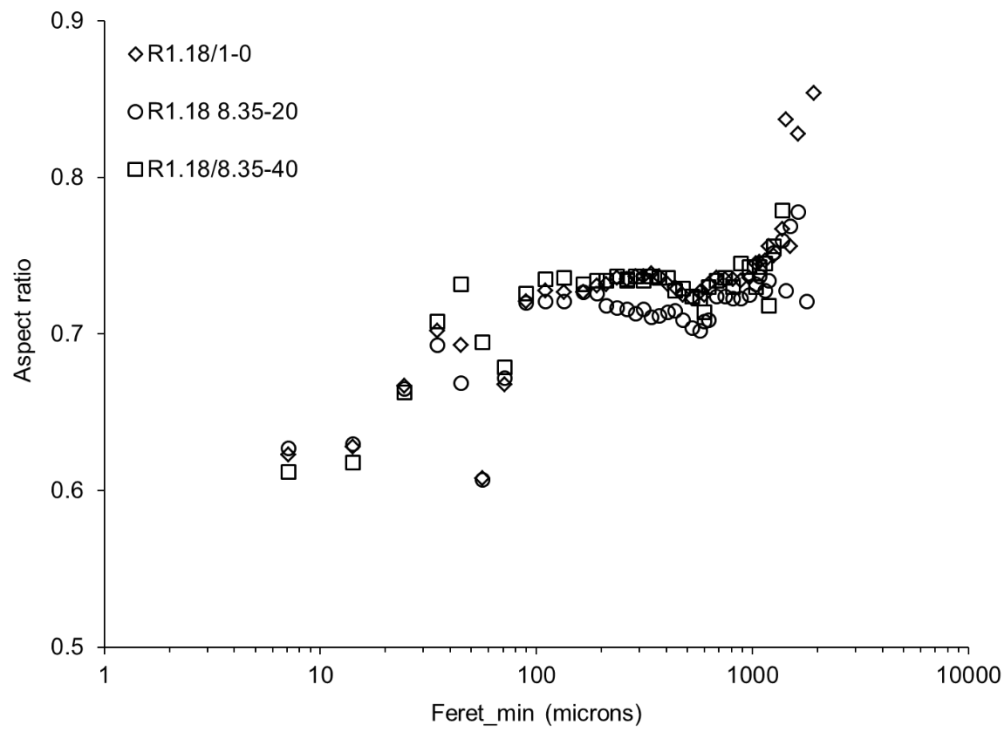**Figure 4** Variation of aspect ratio with size after testing
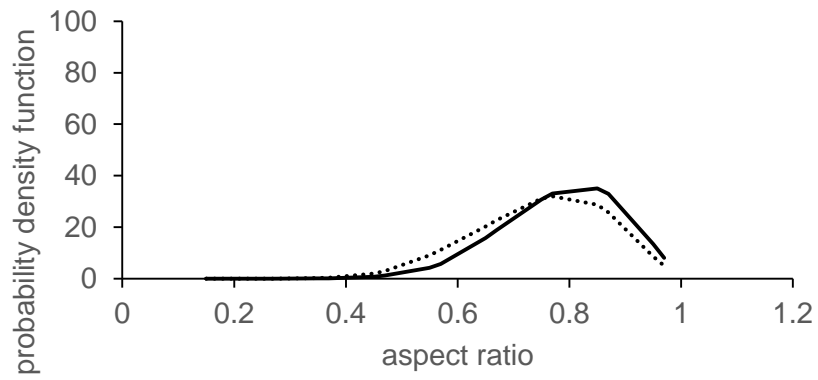
(a)

(b)
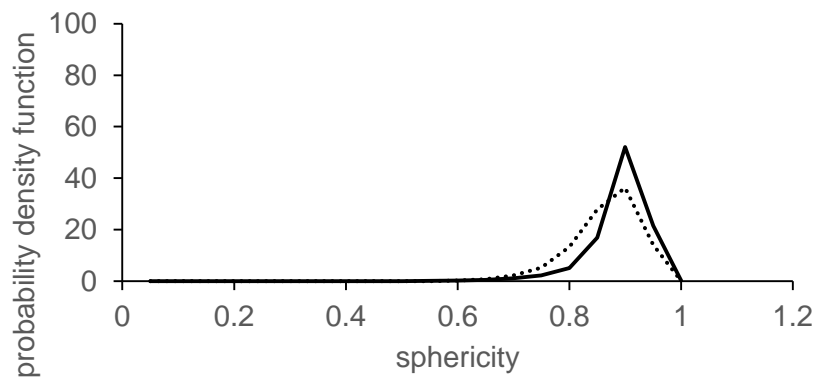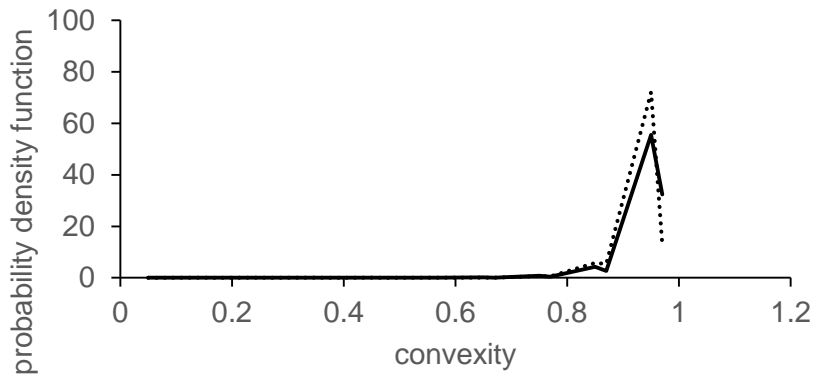
(c)

Figure 5 Probability density functions of particle shapes before and after test for specimens prepared with 40% small grains (R1.18/8.35-40)

(a) R1.18/8.35-20

(b)R2.0/8.78-20

(b) R2.36/8.52-20

Figure 6 Scanning electron micrographs of small sand grains created in zone 2 after test on gap-graded sample with 20% SG content: (a) small and large grains (specimen R1.18/8.35-20); (b) small and large grains (R2.0/8.78-20) and (c) small grains (R2.36/8.52-20).

EQPC	1132.613 μm	
FERET_MAX	1603.915 μm	
FERET_MIN	881.012 μm	
FERET_MEAN	1278.474 μm	
FERET_MAX90	899.556 μm	
FERET_MIN90	1597.621 μm	
BR_MIN	881.012 μm	
BR_MAX	1597.621 μm	
LEFI	1681.401 μm	
DIFI	499.665 μm	
Sphericity	0.816	
Aspect ratio	0.549	
Convexity	0.946	
Elongation	0.297	
Image number	3516	

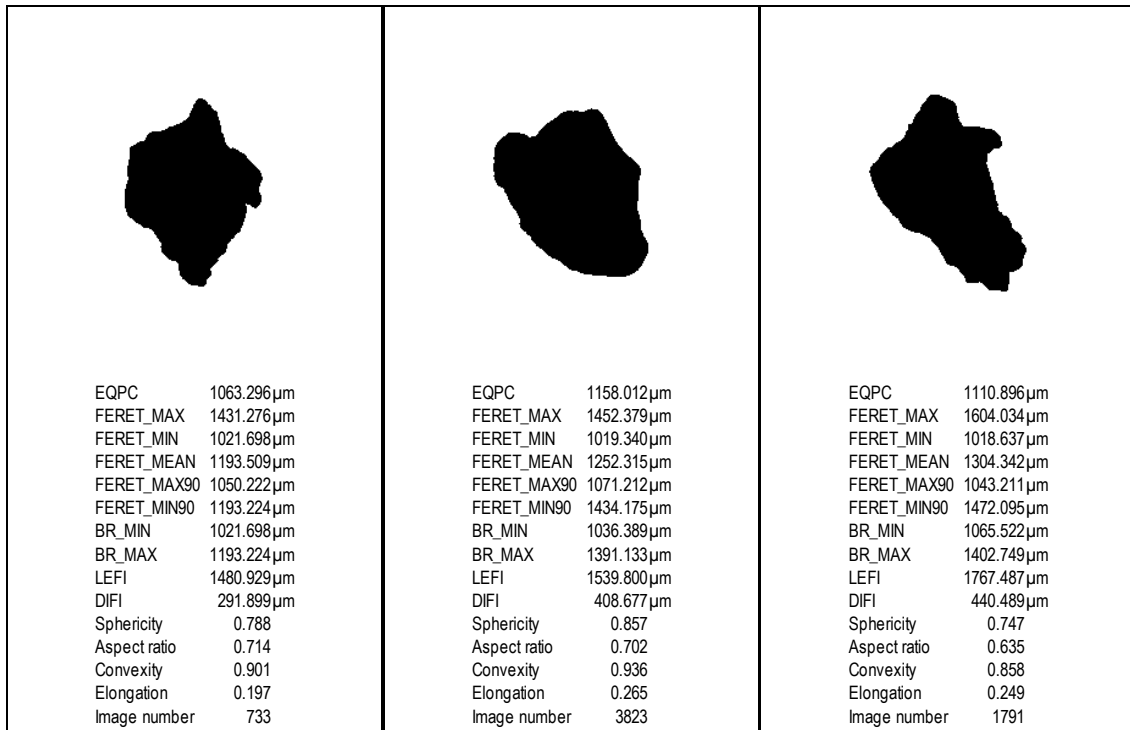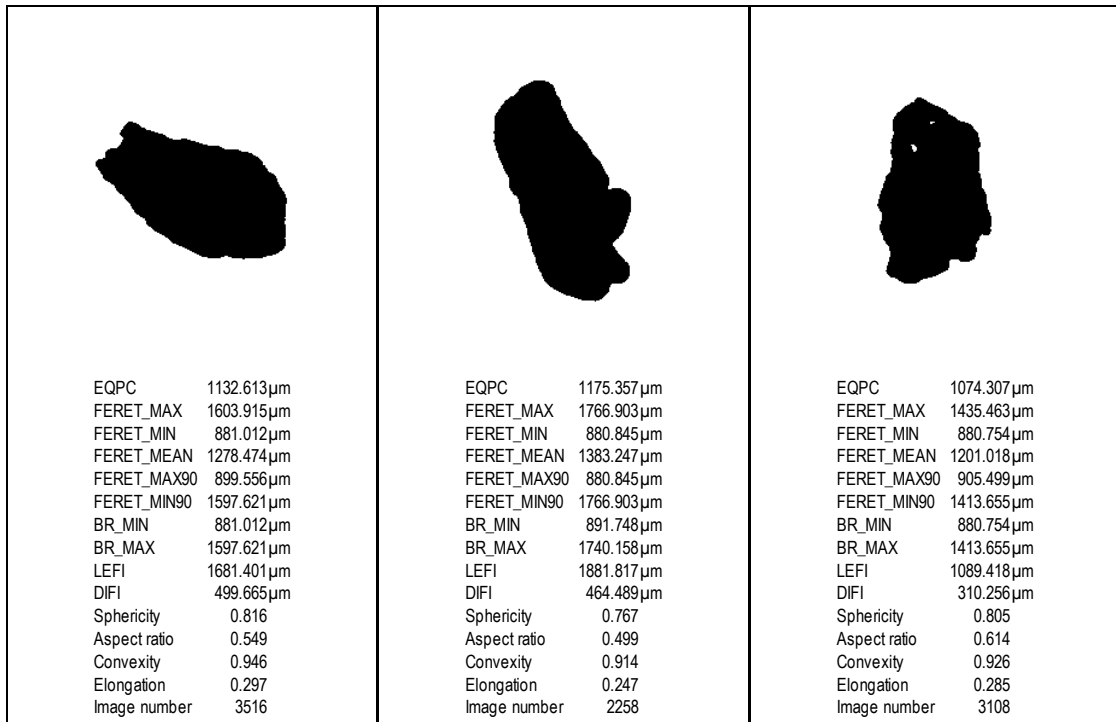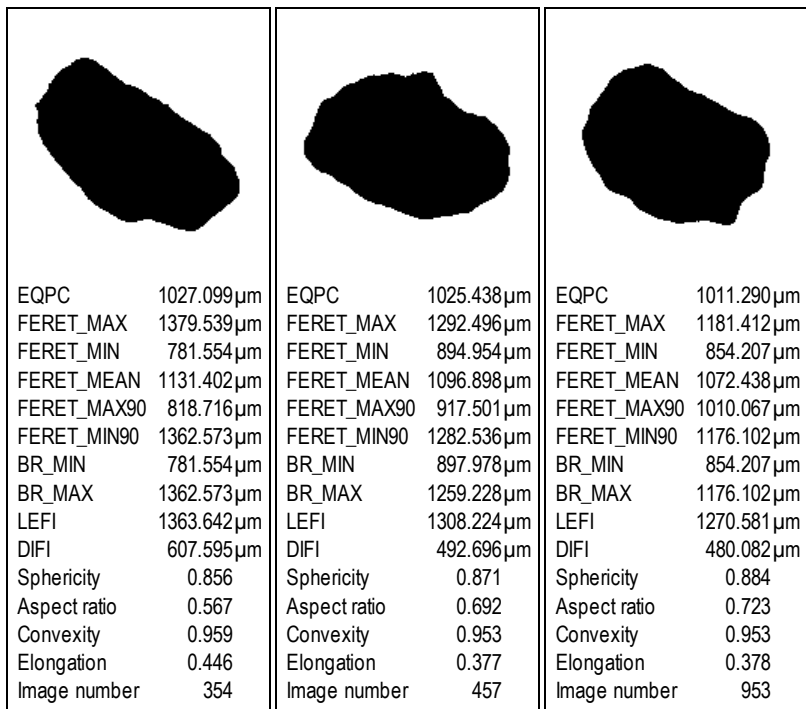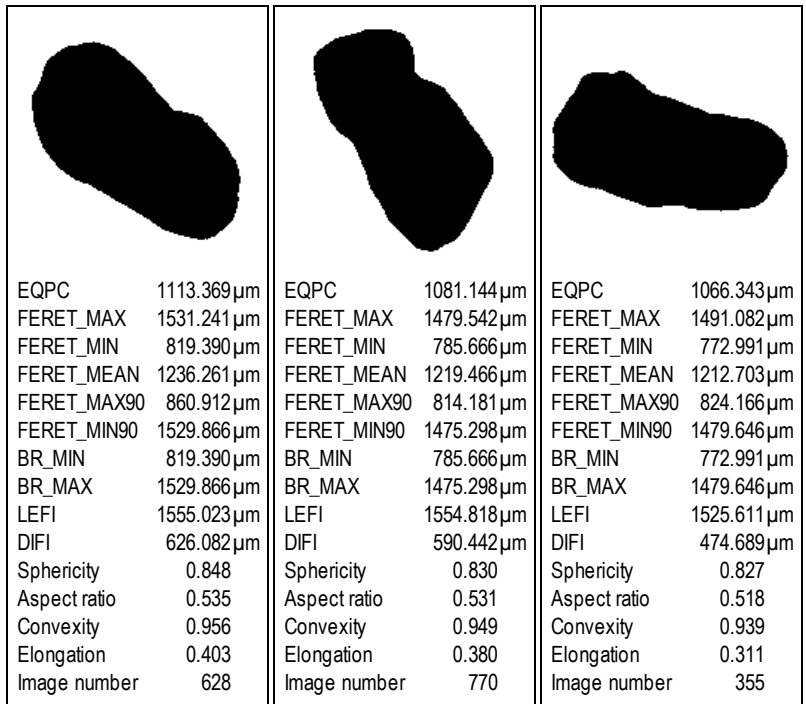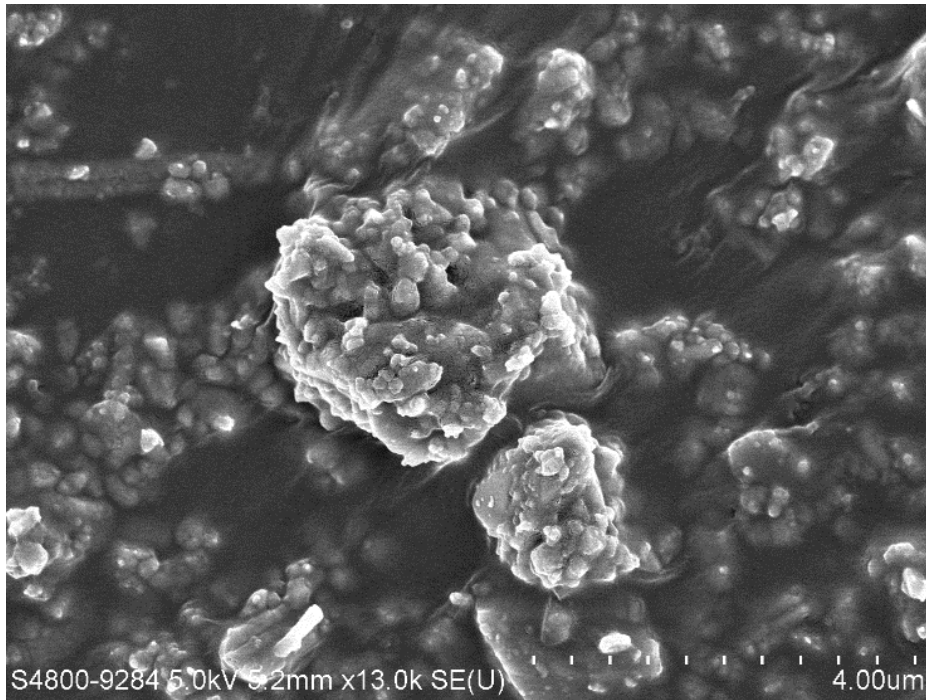|	
EQPC	1175.357 μm
FERET_MAX	1766.903 μm
FERET_MIN	880.845 μm
FERET_MEAN	1383.247 μm
FERET_MAX90	880.845 μm
FERET_MIN90	1766.903 μm
BR_MIN	891.748 μm
BR_MAX	1740.158 μm
LEFI	1881.817 μm
DIFI	464.489 μm
Sphericity	0.767
Aspect ratio	0.499
Convexity	0.914
Elongation	0.247
Image number	2258

EQPC	1074.307 μm
FERET_MAX	1435.463 μm
FERET_MIN	880.754 μm
FERET_MEAN	1201.018 μm
FERET_MAX90	905.499 μm
FERET_MIN90	1413.655 μm
BR_MIN	880.754 μm
BR_MAX	1413.655 μm
LEFI	1089.418 μm
DIFI	310.256 μm
Sphericity	0.805
Aspect ratio	0.614
Convexity	0.926
Elongation	0.285
Image number	3108

EQPC	1063.296 μm
FERET_MAX	1431.276 μm
FERET_MIN	1021.698 μm
FERET_MEAN	1193.509 μm
FERET_MAX90	1050.222 μm
FERET_MIN90	1193.224 μm
BR_MIN	1021.698 μm
BR_MAX	1193.224 μm
LEFI	1480.929 μm
DIFI	291.899 μm
Sphericity	0.788
Aspect ratio	0.714
Convexity	0.901
Elongation	0.197
Image number	733

EQPC	1158.012 μm
FERET_MAX	1452.379 μm
FERET_MIN	1019.340 μm
FERET_MEAN	1252.315 μm
FERET_MAX90	1071.212 μm
FERET_MIN90	1434.175 μm
BR_MIN	1036.389 μm
BR_MAX	1391.133 μm
LEFI	1539.800 μm
DIFI	408.677 μm
Sphericity	0.857
Aspect ratio	0.702
Convexity	0.936
Elongation	0.265
Image number	3823

EQPC	1110.896 μm
FERET_MAX	1604.034 μm
FERET_MIN	1018.637 μm
FERET_MEAN	1304.342 μm
FERET_MAX90	1043.211 μm
FERET_MIN90	1472.095 μm
BR_MIN	1065.522 μm
BR_MAX	1402.749 μm
LEFI	1767.487 μm
DIFI	440.489 μm
Sphericity	0.747
Aspect ratio	0.635
Convexity	0.858
Elongation	0.249
Image number	1791

(a)

EQPC	1113.369 μm	EQPC	1081.144 μm	EQPC	1066.343 μm
FERET_MAX	1531.241 μm	FERET_MAX	1479.542 μm	FERET_MAX	1491.082 μm
FERET_MIN	819.390 μm	FERET_MIN	785.666 μm	FERET_MIN	772.991 μm
FERET_MEAN	1236.261 μm	FERET_MEAN	1219.466 μm	FERET_MEAN	1212.703 μm
FERET_MAX90	860.912 μm	FERET_MAX90	814.181 μm	FERET_MAX90	824.166 μm
FERET_MIN90	1529.866 μm	FERET_MIN90	1475.298 μm	FERET_MIN90	1479.646 μm
BR_MIN	819.390 μm	BR_MIN	785.666 μm	BR_MIN	772.991 μm
BR_MAX	1529.866 μm	BR_MAX	1475.298 μm	BR_MAX	1479.646 μm
LEFI	1555.023 μm	LEFI	1554.818 μm	LEFI	1525.611 μm
DIFI	626.082 μm	DIFI	590.442 μm	DIFI	474.689 μm
Sphericity	0.848	Sphericity	0.830	Sphericity	0.827
Aspect ratio	0.535	Aspect ratio	0.531	Aspect ratio	0.518
Convexity	0.956	Convexity	0.949	Convexity	0.939
Elongation	0.403	Elongation	0.380	Elongation	0.311
Image number	628	Image number	770	Image number	355

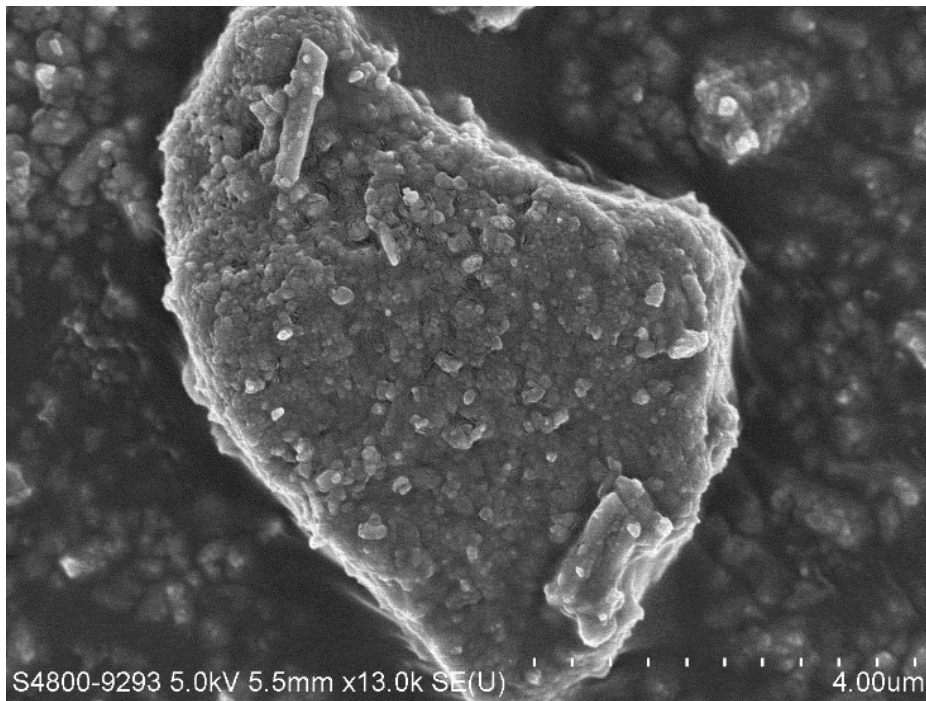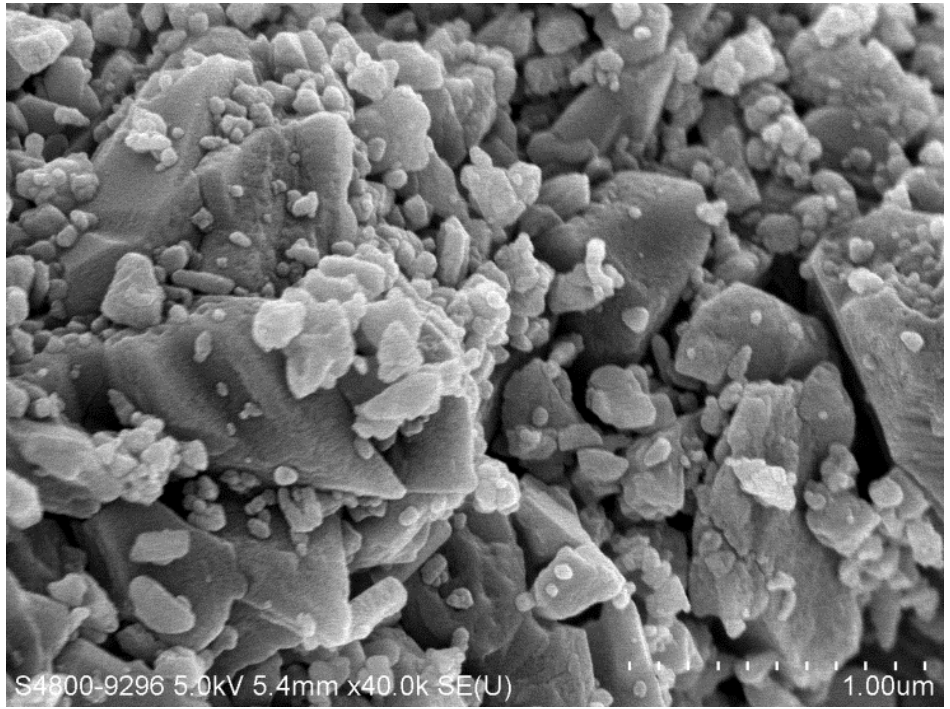| EQPC	1027.099 μm	EQPC	1025.438 μm	EQPC	1011.290 μm
FERET_MAX	1379.539 μm	FERET_MAX	1292.496 μm	FERET_MAX	1181.412 μm
FERET_MIN	781.554 μm	FERET_MIN	894.954 μm	FERET_MIN	854.207 μm
FERET_MEAN	1131.402 μm	FERET_MEAN	1096.898 μm	FERET_MEAN	1072.438 μm
FERET_MAX90	818.716 μm	FERET_MAX90	917.501 μm	FERET_MAX90	1010.067 μm
FERET_MIN90	1362.573 μm	FERET_MIN90	1282.536 μm	FERET_MIN90	1176.102 μm
BR_MIN	781.554 μm	BR_MIN	897.978 μm	BR_MIN	854.207 μm
BR_MAX	1362.573 μm	BR_MAX	1259.228 μm	BR_MAX	1176.102 μm
LEFI	1363.642 μm	LEFI	1308.224 μm	LEFI	1270.581 μm
DIFI	607.595 μm	DIFI	492.696 μm	DIFI	480.082 μm
Sphericity	0.856	Sphericity	0.871	Sphericity	0.884
Aspect ratio	0.567	Aspect ratio	0.692	Aspect ratio	0.723
Convexity	0.959	Convexity	0.953	Convexity	0.953
Elongation	0.446	Elongation	0.377	Elongation	0.378
Image number	354	Image number	457	Image number	953

(b)

Figure 7 Two-dimensional projected images of grains with equivalent perimeter circumference of about 1-1.1mm from specimens prepared with 40% small grains (R1.18/8.35-40) (a) before test; (b) after test

(a)

(b)

(c)

Figure 8 Scanning electron micrographs of small sand grains ($< 63\mu m$) created in zone 2 after test (a) from uniform sample (R2.36/1-0); (b) and (c) from gap-graded sample with 20% SG content (R2.36/8.52-20)
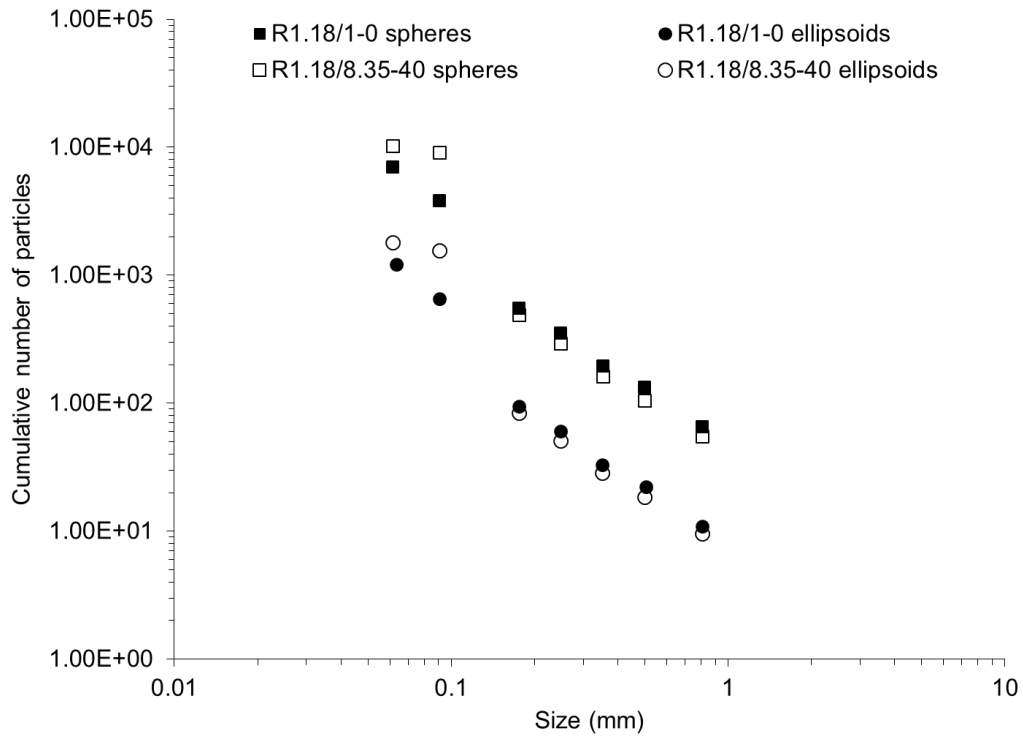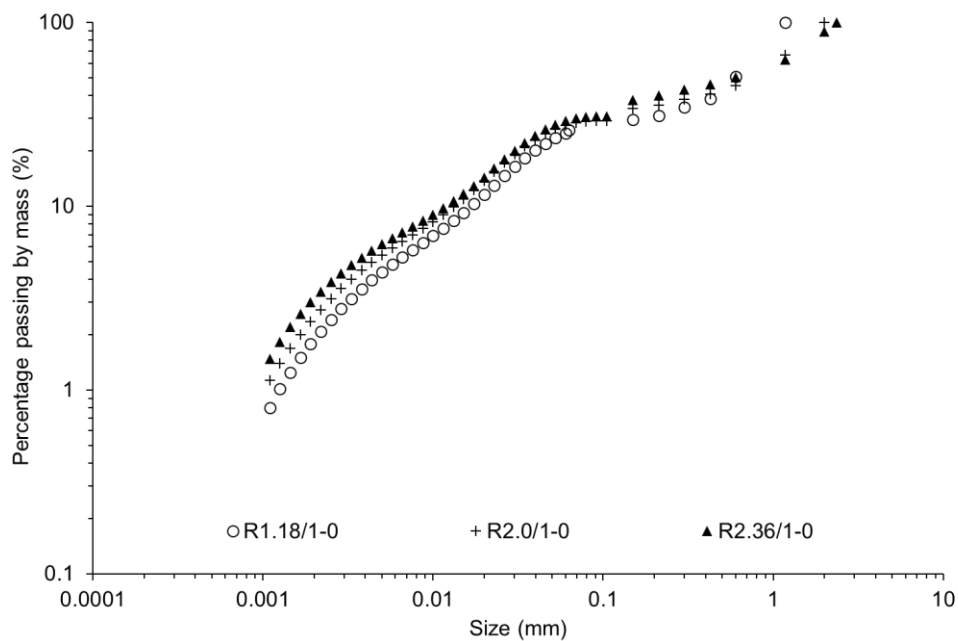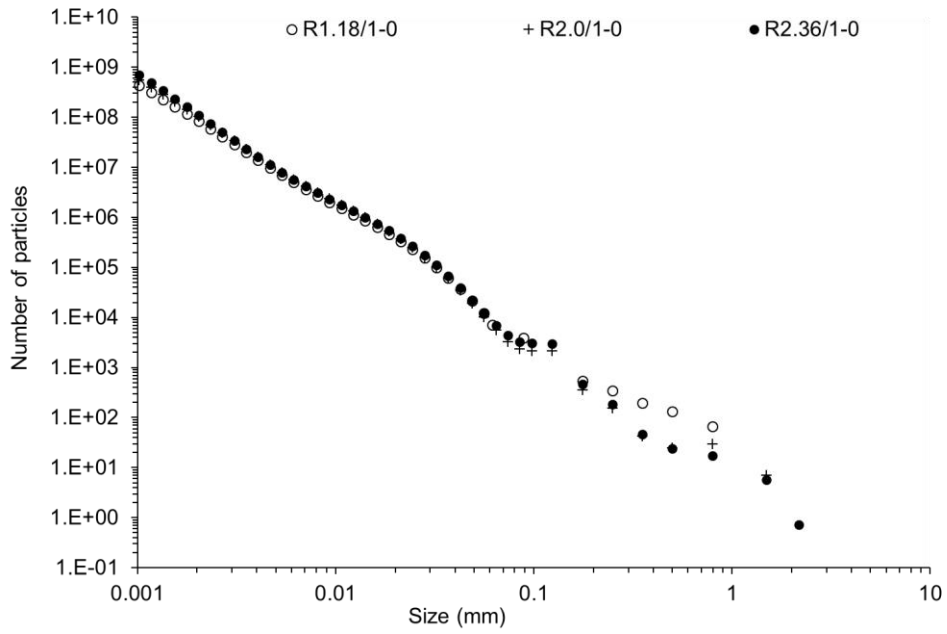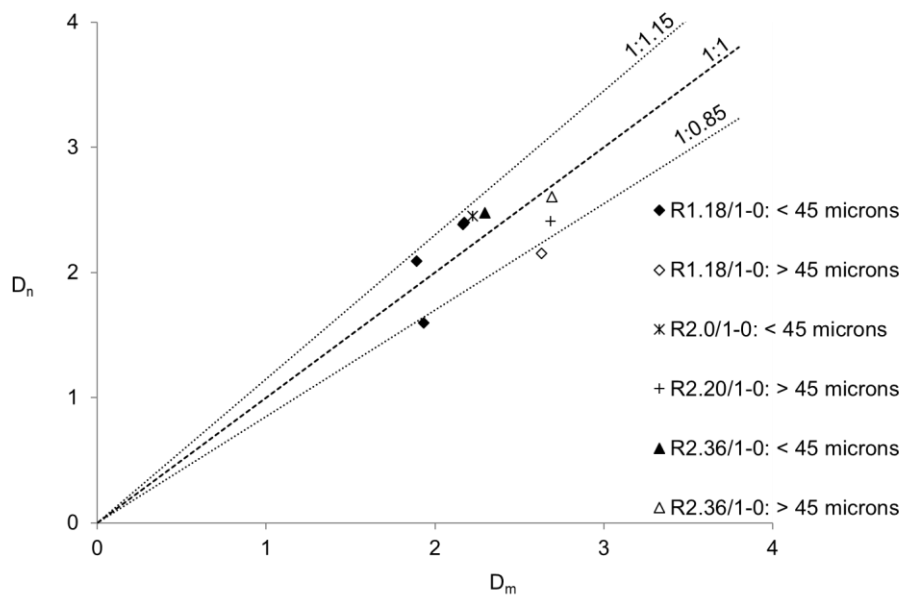
Figure 9 Comparison of number-of-particles size distributions calculated assuming spherical or ellipsoidal grains

(a)

(b)

(c)

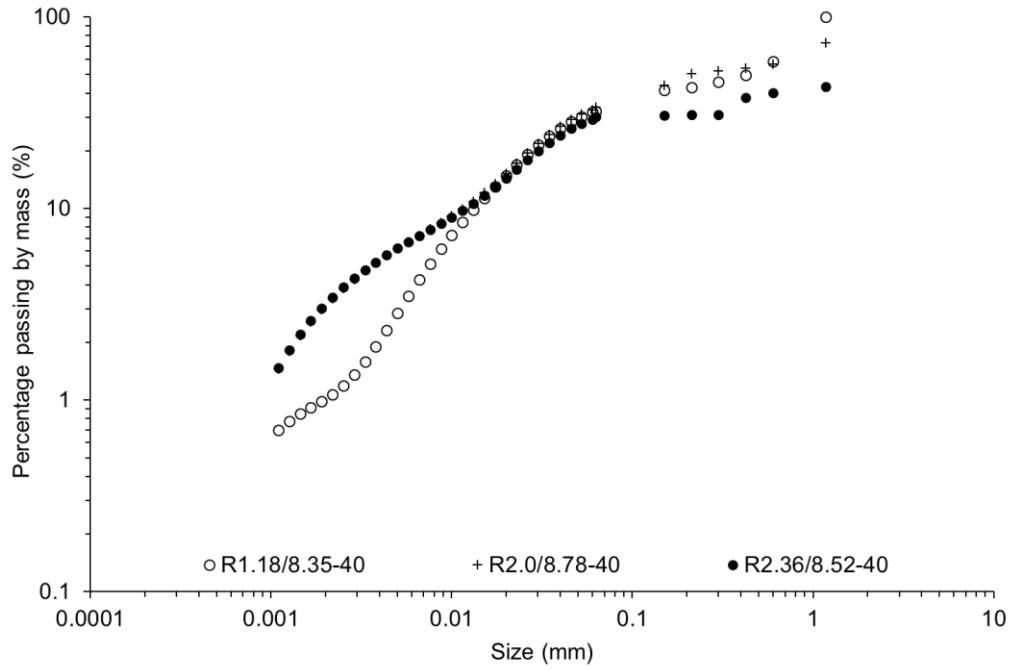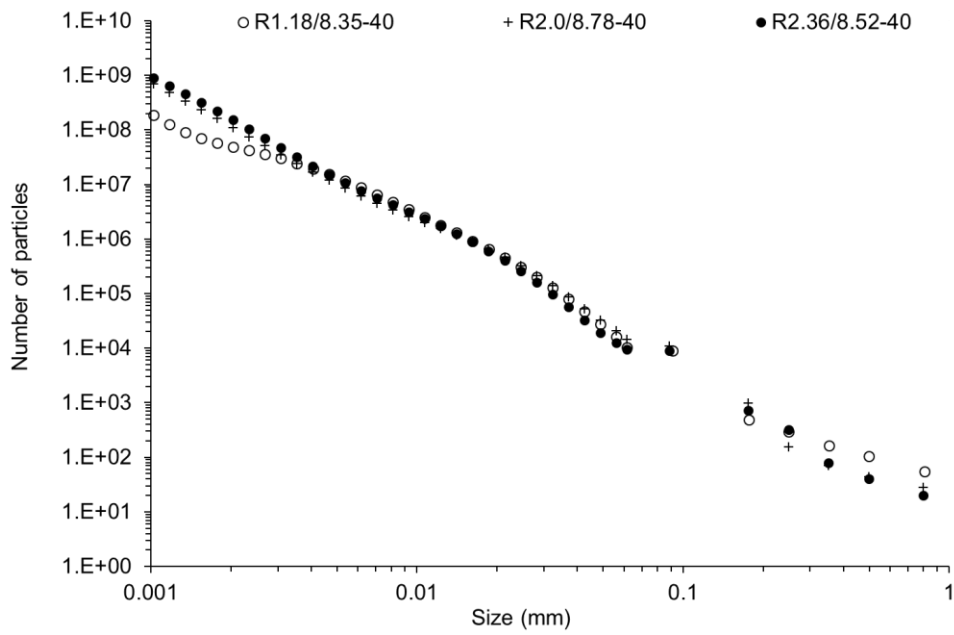**Figure 10** Particle size distribution after shearing the uniform specimens (a) mass cumulative distribution function (b) number-based distribution (c) comparison of fractal dimensions computed by mass-based and number-based approaches

(a)

(b)

Figure 11 Particle size distribution after shearing the specimens prepared with 40% small grains (a) mass cumulative distribution function (b) number-based distribution
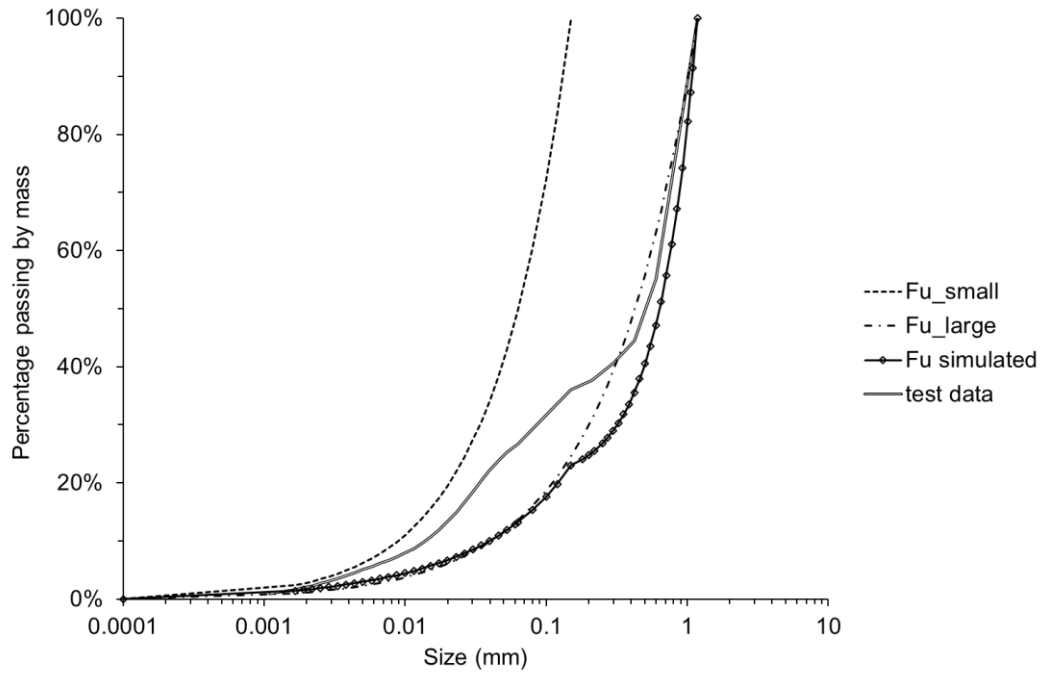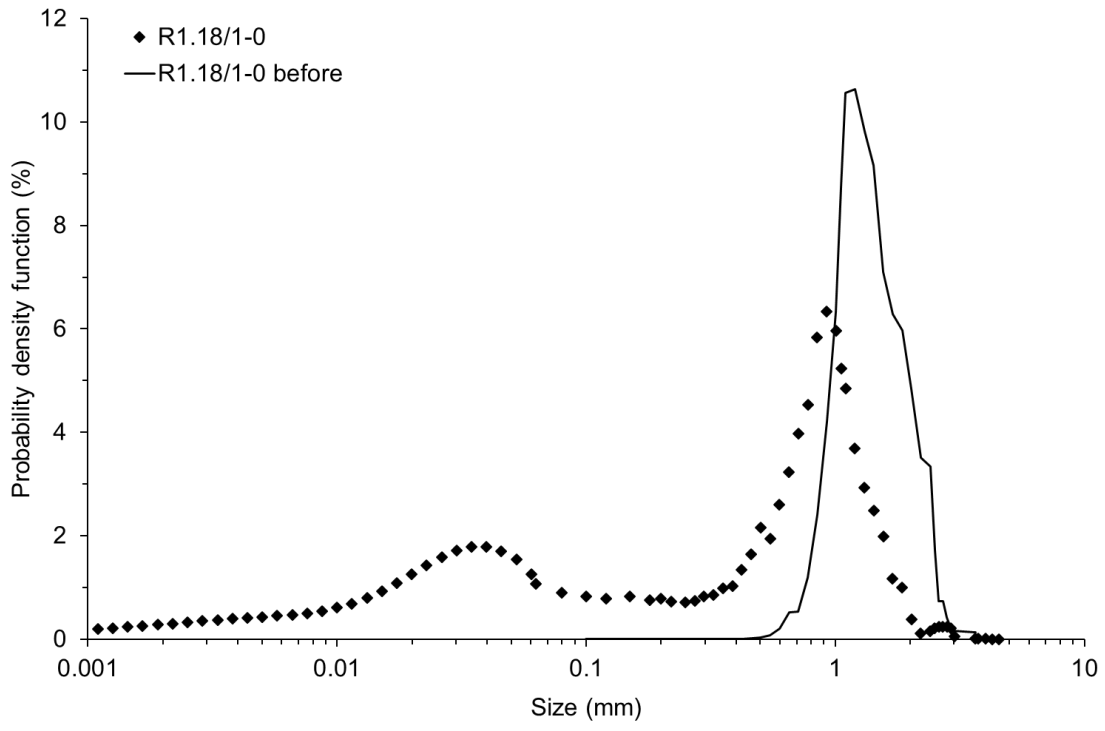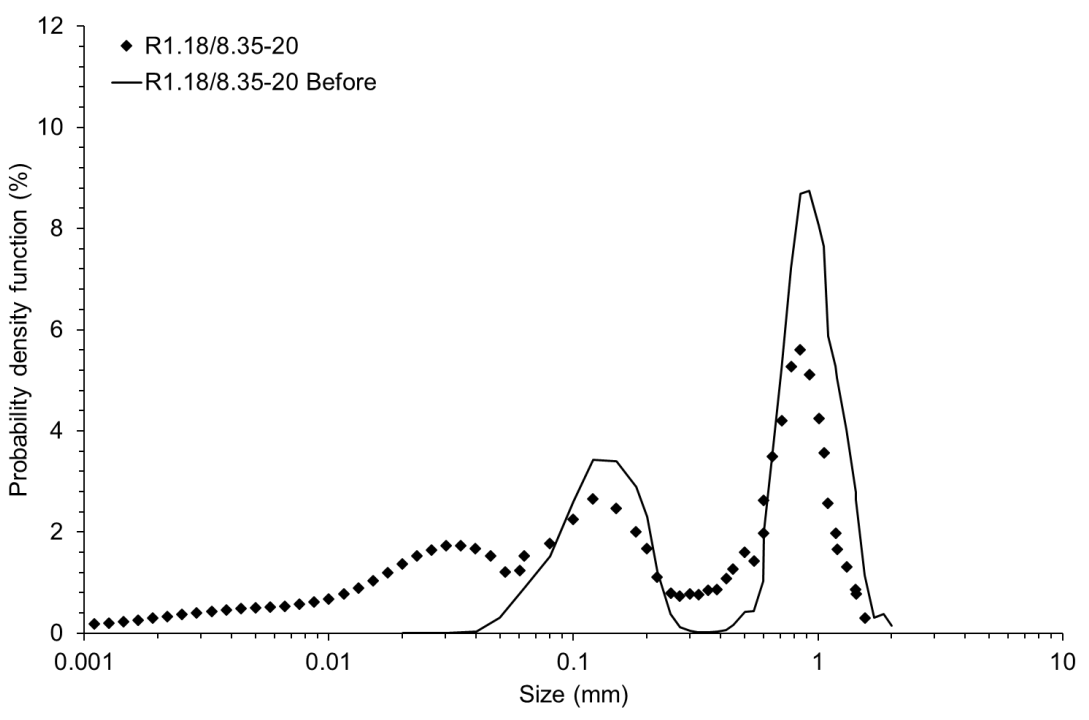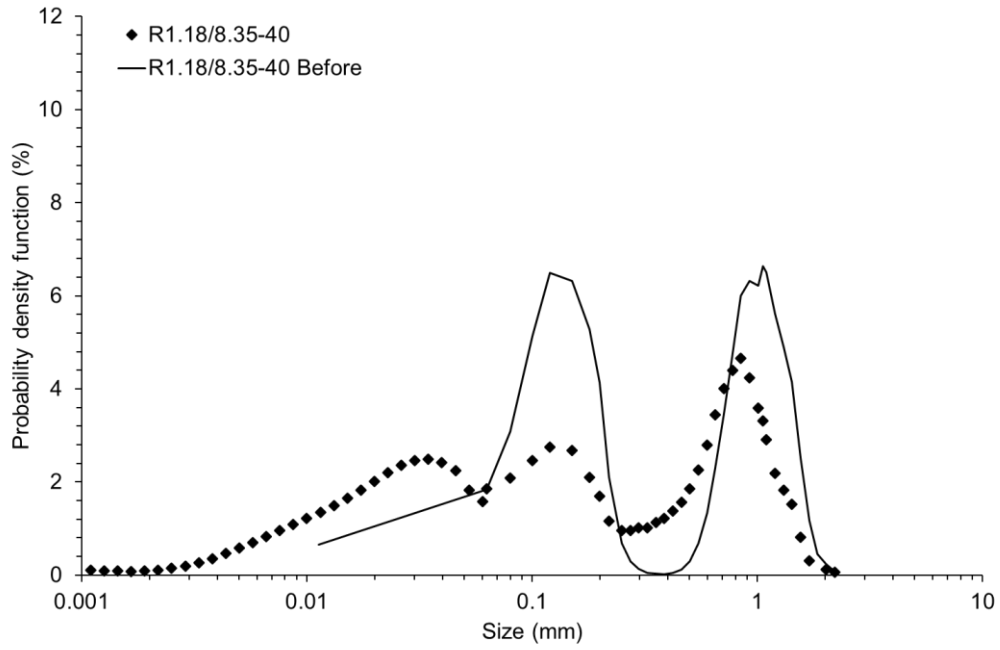
(a)
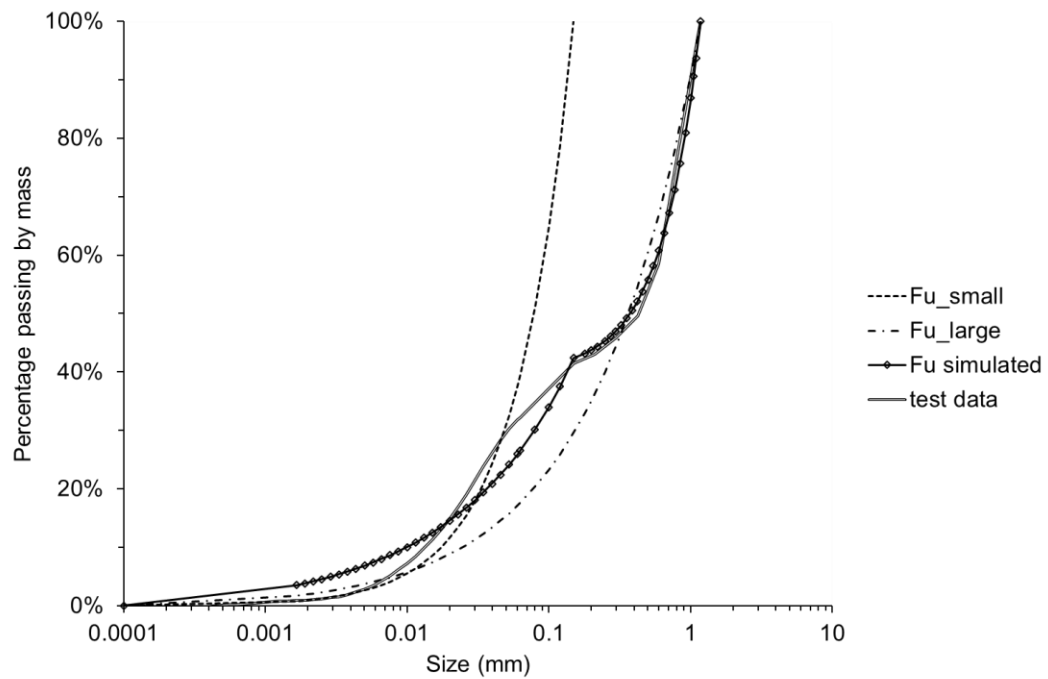
(b)

Figure 12 Predicted mass cumulative distribution functions of specimens R1.18/8.35-20 and R1.18/8.35-40 assuming that the coarse and fine sand fractions tend towards fractal distributions (a) 20% SG; (b) 40% SG content

(a)

(b)

(c)

Figure 13 Probability density functions of particle sizes before and after test for small grains contents of (a) 0%; (b) 20%; (c) 40%